THE JOURNAL OF PHYSICAL CHEMISTRY B

Article

pubs.acs.org/JPCB

Comparison of Acid Generation in EUV Lithography Films of Poly(4-hydroxystyrene) (PHS) and Noria Adamantyl Ester (Noria-AD$_{50}$)

Weiqiang Wu, Kirill Nuzhdin, Mariya Vyushkova, Ireneusz Janik, and David Bartels*

Radiation Laboratory, University of Notre Dame, Notre Dame, Indiana 46556, United States

Supporting Information

ABSTRACT: The mechanism for acid production in phenolic extreme ultraviolet (EUV) lithography films containing triphenylsulfonium triflate ($Ph_3S^+TfO^-$) acid generator has been investigated by electron paramagnetic resonance (EPR) spectroscopy and by use of the acid indicator coumarin 6 (C6). Gamma radiolysis was substituted for the EUV radiation with the assumption that the chemistry generated by ionization of the matrix does not depend on the ionization source. Poly(4-hydroxystyrene) (PHS) was first investigated as a well-studied standard, after which the water-wheel-like cyclic oligomer derivative containing pendant adamantyl ester groups, noria-AD$_{50}$, was investigated. EPR measurements confirm that the dominant free radical product is a phenoxyl derivative (PHS-O$^\bullet$ or noria-O$^\bullet$) that exhibits quite slow stretched exponential recombination kinetics at room temperature. Also observed at 77 K was the presence of a significant hydrogen atom product of radiolysis. The *G* value or yield of acid production in thin lithography films was measured with the C6 indicator on a fused silica substrate. It was found that a significant amount of acid is generated via energy transfer from the irradiated fused-silica substrate to the $Ph_3S^+TfO^-$ in the films. By varying the film thickness on the substrates, the substrate effect on the acid yield was quantitatively determined. After subtraction of the contribution from the substrates, the acid yield *G* value in the PHS film with 10 wt % $Ph_3S^+TfO^-$ and 5 wt % C6 was determined to be 2.5 ± 0.3 protons per 100 eV of radiation. The acid yield of noria-AD$_{50}$ films was found to be 3.2 ± 0.3 protons per 100 eV.

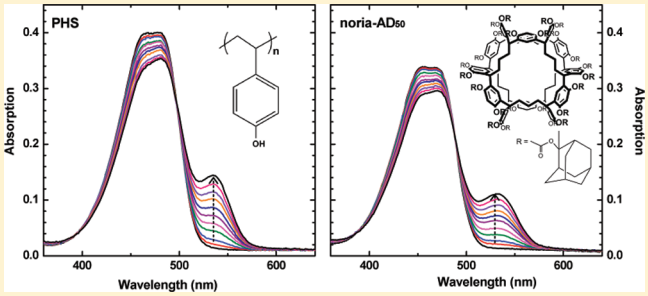

1. INTRODUCTION

The semiconductor industry has been successful for several decades in miniaturizing by orders of magnitude the size of circuit components, making them much cheaper and enormously faster. Photolithography has been a powerful tool for the mass production of semiconductor devices.[1−4] In this technique, the semiconductor is coated with a photosensitive resist material, the resist is exposed to photons in a desired pattern, and this latent image is then developed, exposing the material below in the desired pattern. The pattern can then be further etched or filled as appropriate to build up the semiconductor device layer by layer. As the size of features on semiconductor chips has decreased, ever shorter wavelengths of light have been necessary to provide the pattern resolution.[1−6] Ultimate resolution has now been reached with the use of extreme ultraviolet (EUV) light. Whereas longer-wavelength light excites bound electronic states of the photoresist material, the 92.5 eV photons of (13.5 nm) EUV radiation directly ionize the atoms of the matrix to produce the latent image. Effectively, the boundary between photochemistry and radiation chemistry has been crossed.[7]

Naturally, the resolution (characterized by line edge roughness, or LER) that can be obtained depends on the photochemical process and resist material as well. High molecular weight of resist polymers,[8−10] polymer molecular weight distribution, and polymer aggregation[11] are the main contributions to poor lithographic performance as these relate to inhomogeneous dissolution rates due to chain entanglement and grain boundaries of various sizes. Over the past decade, there has been considerable research in the utilization of molecular glass photoresists for EUV lithography.[12] These materials are composed of building blocks that are monodisperse and may be as much as an order of magnitude smaller in size. The reduction of the grain size is believed to be a fundamental improvement in the ability to consistently obtain low LER. Recently, Kudo et al. have successfully synthesized a new ladder-type cyclic oligomer from resorcinol and 1,5-pentanedial in a one-pot procedure.[13] This oligomer has 24 hydroxyl groups, 6 cavities in the side, and a large hydrophobic hole through the center of the molecule, giving an average radius of 2 nm.[13] The molecule resembles a water wheel; therefore, it was named noria, meaning water wheel in Spanish. Although noria itself does not form good lithography films by spin-coating, some ester derivatives of the noria molecule work well, where the ester groups also act as acid deprotectable sites necessary for inducing a solubility switch. When 50% of the total hydroxyl groups in noria are substituted by 2-acetyloxy-2-methyladamantyl ester groups (AD), giving noria-AD$_{50}$

Received: January 19, 2012
Revised: April 20, 2012
Published: May 18, 2012

   dx.doi.org/10.1021/jp300677q | *J. Phys. Chem. B* 2012, 116, 6215−6224

(Scheme 1), clear line and space patterning could be obtained with resolutions of 26−40 nm in EUV lithography.[14−17] We

Scheme 1. Structures of PHS and Noria-AD$_{50}$

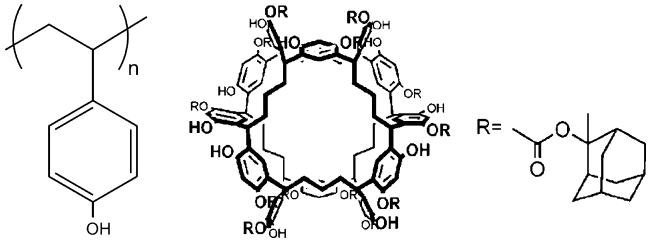

have undertaken a study of the radiation chemistry mechanism of noria-AD$_{50}$ lithographic films to test its photochemical efficiency with respect to traditional resist matrix materials based on poly-(4-hydroxystyrene) (PHS).

To provide better sensitivity of the photochemical process, thereby decreasing exposure times and cost, chemically amplified resist technology has been widely adopted in the industry. Chemically amplified resists utilize acids generated by light exposure to catalyze deprotection reactions that alter the solubility of resist materials.[6,18] Chemical efficiency in the development step depends on how many deprotection reactions can be catalyzed per photogenerated proton when the exposed resist is briefly heated in the post exposure bake. This number is necessarily limited because diffusion of any proton over a large distance to catalyze many reactions will degrade the pattern resolution. A more immediate measure of the photochemical efficiency is the radiation chemistry G value, the number of labile acid protons produced per unit of absorbed radiation energy.

A widely used lithography system makes use of the salt triphenylsulfonium triflate ($Ph_3S^+TfO^-$) as a photoacid generator in concert with phenolic polymers. On the basis of numerous previous studies, we can predict the following outline for radiolytic chemistry in this system[19−21]

$$\text{Matrix} + \text{radiation} \rightarrow \text{hole}^+ + e^- \quad (1)$$

$$e^- + Ph_3S^+ \rightarrow Ph_2S + Ph^\bullet \quad (2)$$

$$\text{hole}^+ \rightarrow -(ArOH^{\bullet+}) \quad (3)$$

$$-(ArOH^{\bullet+}) + -(ArOH) \rightarrow -(ArO^\bullet) + -(ArOH_2^+) \quad (4)$$

$$Ph^\bullet + -(ArOH) \rightarrow PhH + -(ArO^\bullet) \quad (5)$$

Energy is deposited mostly in the phenolic resist matrix material due to its larger electron fraction of the material. A charge pair consisting of a matrix radical cation and an ejected electron is generated (reaction 1). The electron is efficiently scavenged (reaction 2) by the photoacid generator, in this case $Ph_3S^+TfO^-$, present at ∼10% weight fraction. The reduced triphenylsulfonium cation dissociates irreversibly to diphenyl sulfide and a phenyl radical. In PHS, the holes localize on the sites of the lowest ionization potential, the phenol rings (reaction 3). Similarly, the holes in noria-AD$_{50}$ are localized on the substituted resorcinol rings. In both PHS and noria-AD$_{50}$ films, the strongly acidic radical cations will transfer a proton to another matrix site (reaction 4), leaving a substituted aryloxy radical. (The pK_a value of the phenol radical cation is reported to be −8.1.[22] We indicate $-(Ar-OH_2^+)$ as the matrix proton acceptor in reaction 4, but any proton acceptor hydrogen-bonded to $-(Ar-OH^+)$ will do.) The counterion of the proton produced in this way is the triflate anion, TfO^-. Triflic acid is a superacid with pK_a on the order of −15; therefore, the proton remains in the matrix, ready to catalyze deprotection reactions.[23] Meantime, the highly reactive phenyl radical can be expected to react by hydrogen abstraction at some site in the matrix, giving another aryloxy radical (reaction 5) or a carbon-centered aliphatic radical.

Because this chemical system depends only on the production of low-energy electrons and holes in the ionization step, its fundamental efficiency can be tested with electron beam, EUV, or γ-radiation with equal facility.[24] (However, the G values may not be identical because the spectrum of secondary electron energies will differ somewhat.) The advantage of γ-radiation is its extreme penetrating power, which ensures a completely uniform irradiation of a sample. EUV or low-energy electron beams, on the other hand, will deposit energy very near a vacuum/film interface, and saturation effects are very likely.

In this study, we have used γ-irradiation and EPR detection to characterize the free radicals generated in both PHS and noria-AD$_{50}$ films formed with $Ph_3S^+TfO^-$ acid generator. Acid indicator molecule coumarin 6 (C6) has been added to the films to provide an in situ measurement of the acid production efficiency.[25,26] As a model for a chemically amplified resist, PHS films have been extensively investigated by Tagawa and co-workers.[19,20,25] This material has the advantage of being cheap and commercially available. The G value of the acid generation efficiency in PHS films containing 4.5 wt % $Ph_3S^+TfO^-$ was previously evaluated to be 2.3 protons per 100 eV of radiation using γ-rays from ^{60}Co.[20] In order to test the accuracy of the C6 indicator method with γ-radiolysis, the PHS films were selected as the resist to be studied first.

2. EXPERIMENTAL SECTION

Model resist polymer poly(4-hydroxystyrene) (PHS; MW: 11000), acid generator triphenylsulfonium triflate ($Ph_3S^+TfO^-$), and acid-sensitive dye coumarin 6 (C6) were purchased from Aldrich Chemical and used without further purification. Casting solvent HPLC-grade tetrahydrofuran (THF, Fisher Scientific) was distilled from sodium three times to remove residual water and peroxides before use. The other resist matrix, noria-AD$_{50}$, was provided as a gift from JSR Micro Inc.[16,17]

The resist polymer PHS or noria-AD$_{50}$, acid generator $Ph_3S^+TfO^-$, and C6 were dissolved in THF with the weight ratio of 10/1/0.5 to form casting solutions. The concentration of resist PHS or noria-AD$_{50}$ is 5 wt % in THF. The solutions were spin-coated onto 1 mm thick, 2.5 cm diameter UV-grade fused silica substrates at 1000 rpm for 30 s and then prebaked at 70 °C for 120 s to evaporate the remaining THF solvent inside of the films. The film thickness was calibrated with a tapping-mode AFM (Veeco Bioscope II) by scraping a film and measuring the edge depth. Several edges were measured on films whose absorption had been measured. The typical film thicknesses of PHS and noria-AD$_{50}$ from the nominal casting solutions were 0.80 and 0.50 μm, respectively. The typical uncertainty of the film thickness was 0.05 μm. The film thickness was changed by diluting the original solution with THF. We did not explore the effect of film roughness and its

dx.doi.org/10.1021/jp300677q | J. Phys. Chem. B 2012, 116, 6215−6224

dependence on the type of spin-casting solvent. The THF was used exclusively because of its good solubility of noria-AD_{50} as opposed to the other typical casting solvents. The relative thickness on the silica substrate was easily determined by the visible absorbance of the C6 indicator prior to irradiation. Absorbance was 5.0×10^3 cm^{-1} at 480 nm for PHS films and 6.0×10^3 cm^{-1} at 460 nm for noria-AD_{50} films.

The films were irradiated with γ-rays from a ^{60}Co source with dose rate of 0.24 kGy min^{-1} in a sealed flask under argon. Some initial experiments and diagnostic experiments were carried out in air as described below. The absorbed dose was determined using an aqueous Fricke dosimeter.[27] The UV−vis spectra of the films after exposure were recorded with a Varian-Cary 50 Bio spectrophotometer to quantify the acid yields by means of the characteristic absorption of C6 and its proton adduct $C6H^+$.[25,26]

The spectra and extinction coefficient of the C6 indicator change slightly depending on the local environment. In Figure 1, we plot spectra of the indicator in THF solution, in the PHS

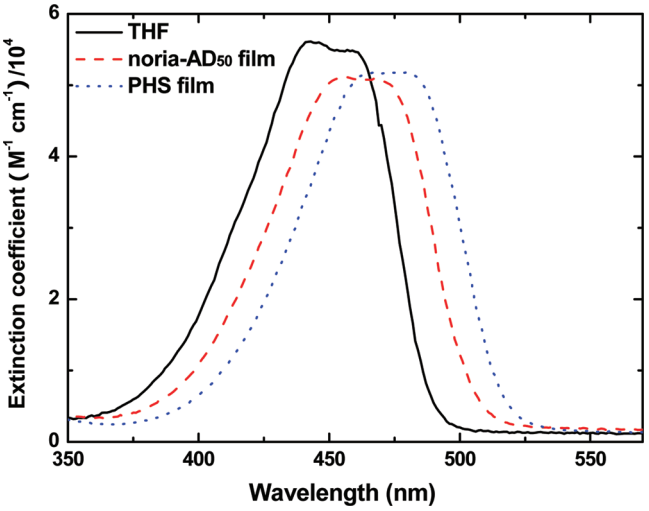

Figure 1. Absorption spectra of C6 in THF solvent, PHS film, and noria-AD_{50} film at room temperature.

film, and in the noria-AD_{50} film. The absolute extinction coefficient is easily calibrated by the known concentration and path length in THF solution. We obtain 5.4×10^4 M^{-1} cm^{-1} in the THF solution, which agrees very well with 5.6×10^4 M^{-1} cm^{-1} determined by Pohlers et al.[26] To place the film spectra on the same absolute scale, it is assumed that total oscillator strength of the transitions, integrated between 350 and 550 nm, are conserved independent of the local environment. As can be seen in Figure 1, the solution spectrum is slightly narrower, and the extinction coefficient of C6 in the films is therefore determined to be 4.9×10^4 M^{-1} cm^{-1}, ~10% lower than that in solution. Correspondingly, the extinction coefficient of the acid form $C6H^+$ in films is extrapolated to be 10% lower than that in solution too. On the basis of the extinction coefficient 9.9×10^4 $M^{-1}cm^{-1}$ of $C6H^+$ reported by Pohlers et al.,[26] it is determined to be 9.0×10^4 M^{-1} cm^{-1}.Yamamoto et al. have used 7.8×10^4 M^{-1} cm^{-1} for C6 in PHS films but do not state the source of this number.[25]

Given a film thickness and extinction coefficient, by assuming Beer's law, we can obtain the molar concentration of the C6 indicator in the films. This is easily converted to the mass density of C6, and from the mass fraction of C6 in the casting solution, we obtain the overall film density. (By dissolving a baked film back into THF and measuring its UV absorbance, we confirmed that the composition of the film is the same as the original casting solution.) The density of the standard PHS film is 1.2 g cm^{-3}, and that of noria-AD_{50} is 1.1 g cm^{-3}. Assuming that the electron density is virtually proportional to the mass density, the absorbed γ-energy can now be calculated relative to the Fricke dosimeter solution.

EPR experiments were carried out on the standard film casting mixtures after evaporating the THF and then loading the powder into a fused silica EPR tube. Irradiations were carried out at 77 K, and then, the tubes were transferred to the spectrometer. First-derivative X-band EPR spectra at room and low temperature (77 K) were measured on a Bruker ER100 spectrometer with its own data acquisition system. For yield measurements, total free radical spins of a sample completely contained inside of the EPR cavity were integrated on a calibrated Bruker EMX plus 10/12 spectrometer. The sample mass was determined by the difference of weight before and after cleaning out the sample tube. The *G* value is simply the number of spins divided by the sample mass and then divided by the dose.

3. RESULTS

3.1. Radical Generation in EUV Film Materials. The EPR spectra observed after γ-radiolysis of PHS and noria-AD_{50} mixed with 10 wt % $Ph_3S^+TfO^-$ and 5 wt % C6 at 77 K are shown in Figure 2a and b, respectively. In both cases, the spectra are dominated by a broad singlet in the center (g = 2.00) region and an unmistakable H atom doublet with hyperfine splitting of ~500 G. Also visible is the narrow silica sample tube E′ signal near g = 2.00,[28] which is a useful internal frequency marker.

The broad singlet signal is consistent with the expected substituted aryloxy radicals. The phenoxyl radical was first observed in the 1950s,[29] and several substituted phenoxyl radicals have been well-characterized with EPR spectroscopy.[30,31] Using the fused quartz E′ signal as an internal standard, the g factor of the substituted phenoxyl radical in PHS was found to be 2.00421, which is identical with one determined previously.[31] The g factor of noria-$O^\bullet$ in noria-AD_{50} was determined to be 2.00451, which is very close to the g factor of 2.00435 ± 0.00015 for the similar structure of the resorcinol radical.[28,32,33] While we might expect to see an additional signal from the phenyl radical (triplet with a = 1.74 mT and a g factor close to 2.00237)[34] formed in Ph_3S^+ decomposition, there is no signal from this radical. Because phenyl radicals are very reactive species, they may abstract H atoms from the matrix even at 77 K.[35,36]

Yields of the aryloxy radicals in noria-AD_{50} and PHS at 77 K were measured from double integration of the spectra to be 5.7 ± 0.5 and 7.0 ± 0.6 per 100 eV, respectively, for a 12 kGy dose. The H atom signal was also integrated, but a large and somewhat variable yield from the empty sample tube (on the order of 50% of the filled sample tubes) makes it difficult to quantify the yield in the film material. The H atom yields were approximately 0.30 ± 0.15 per 100 eV. Upon warming the samples from 77 K to room temperature, the H atoms disappeared, and aryloxy radical yields decreased dramatically to 0.4 ± 0.04 per 100 eV in PHS and to 0.9 ± 0.1 per 100 eV in noria-AD_{50}.

The aryloxy radicals in both PHS and noria-AD_{50} decayed relatively slowly at room temperature in the sealed sample

dx.doi.org/10.1021/jp300677q | J. Phys. Chem. B 2012, 116, 6215−6224

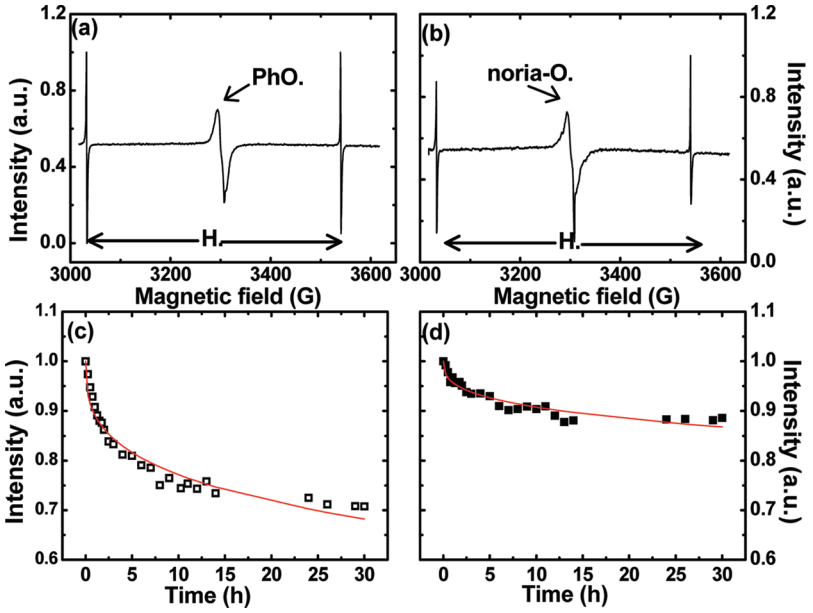

Figure 2. First-derivative EPR spectra after γ-radiolysis of PHS and noria-AD_{50} with $Ph_3S^+TfO^-$ (10 wt %) and a C6 (5 wt %) mixture in a quartz tube at 77 K: (a) PHS; (b) noria-AD_{50}. (c,d) Kinetics of the phenoxyl radicals in PHS and noria-AD_{50} at room temperature; points fitted by stretched exponential functions, $I(t) = \exp[-(2.2 \times 10^{-3}t)^{-0.35}]$ for PHS and $I(t) = \exp[-(1.2 \times 10^{-4}t)^{-0.35}]$ for noria-AD_{50} (for t given in hours).

tubes. Figure 2c and d shows the decay of aryloxy radicals in both PHS and noria-AD_{50} at room temperature. The decay arises from recombination reactions, for example, cross-linking or rearrangement followed by combination of phenoxy radicals generating cross-linked quinone-type structures.[37] As shown in Figure 2c and d, the decay rate of noria-$O^\bullet$ is slower than that of PHS-$O^\bullet$ at room temperature. Possibly, steric hindrance arising from bulky adamantyl groups prohibits the radical recombination and rearrangement and thus prolongs the noria-$O^\bullet$ lifetime. Decay kinetics in glassy systems such as these almost universally follow a stretched exponential form,[38−41] $I(t)/I(0) = \exp[-(kt)^\beta]$. The aryloxy radical decay follows this form qualitatively, as illustrated in Figure 2c and d, but a close examination of the fit shows significant deviation at short time. It seems most likely that this deviation reflects the formation and decay of geminate pairs of aryloxy radicals in the reactions 4 and 5 suggested above.

H atoms are a common product of hydrocarbon radiolysis, often giving rise to H_2 product when H-abstraction reactions become thermally accessible at higher temperature. In the present case, we suggest that the H atom could largely be generated from the direct O−H bond fission of electronically excited phenol units in PHS and noria-AD_{50}.[42,43] This process will also generate some of the observed aryloxy radical signal, as mentioned above. Upon warming above 100 K, the H atoms become mobile and disappear. We can expect that this occurs both via recombination with aryloxy radicals and via second-order production of H_2. For irradiations at room temperature, the H atoms should also be formed from the phenol excited states. However, their decay might be dominated at room temperature by thermally activated addition to the aromatic phenol rings, giving initially a hydroxycyclohexadienyl radical. This radical could probably decay by elimination of H_2, giving once again the lowest-energy aryloxy radical.

An alternative radiolysis mechanism that might contribute to the chemistry in noria-AD_{50} is electron capture by the ester groups.[44] Sevilla and co-workers were able to see ester anion radicals in aqueous glasses at 77 K and observe their fragmentation reactions upon warming above 120 K. Typically, beta scission occurs to give the carboxylate anion and an alkyl radical. In the noria-AD_{50} case, one might expect a noria carboxylate anion and 2-methyladamantyl radical. To the extent that electron capture at the ester occurs, this process will reduce the labile proton generation efficiency because the acid anion product is a much stronger base than the TfO^- anion corresponding to Ph_3S^+ annihilation. Noria-AD_{50} was irradiated at 77 K without the addition of $Ph_3S^+TfO^-$. The resulting EPR spectrum is essentially identical to the spectrum shown in Figure 2b. The same broad singlet spectrum ascribed to noria-$O^\bullet$ is observed, with no evidence of any second radical. Any H atom yield was too small to measure in the presence of the sample tube signal. Integration of the spectrum gives a G value of 1.6/100 eV for the noria-$O^\bullet$. This is significantly lower than the G value of 5.7/100 eV in the presence of 10% $Ph_3S^+TfO^-$. If the noria-$O^\bullet$ comes from excited-state O−H bond fission, it implies that second-order recombination of H atoms to H_2 is much more probable than recombination with noria-$O^\bullet$. We conclude that if electron capture occurs at the ester group in the noria-AD_{50} matrix, its cross section is considerably below the cross section for capture by Ph_3S^+. Nevertheless, there is evidence that the process occurs because some acid generation is observed in the absence of $Ph_3S^+TfO^-$. This is discussed in section 3.5 below.

3.2. Acid Generation Efficiency of PHS Films under an Argon Atmosphere. The PHS films prepared on fused silica windows with 10 wt % $Ph_3S^+TfO^-$ and 5 wt % C6 were put into a glass flask, sealed with a rubber septum, and then purged with argon using hypodermic needles inserted through the septum. The flasks with PHS films were irradiated with ^{60}Co γ-rays at "room temperature", which is ~30 °C inside of the γ-source. The acid-sensitive dye C6 was used to quantify the acid generated in the films. It has been reported that the neutral form and proton adduct of C6 show characteristic absorption bands at 460 and 533 nm, respectively.[25,26] Figure 3a shows representative absorption spectra of PHS films with $Ph_3S^+TfO^-$ and C6 before and after γ-ray exposure. Under radiolysis, labile

dx.doi.org/10.1021/jp300677q | J. Phys. Chem. B 2012, 116, 6215−6224

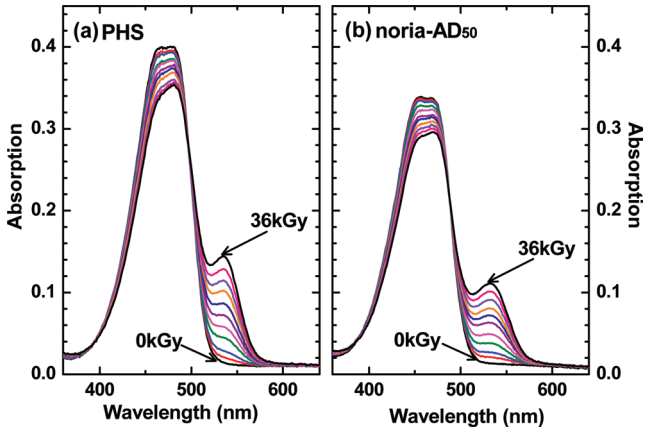

Figure 3. Absorption spectra of (a) PHS and (b) noria-AD_{50} films with 10 wt % $Ph_3S^+TfO^-$ and 5 wt % C6 with increasing γ-rays exposure. Doses are 0, 2, 4, 8, 12, 16, 20, 24, 28, 32, and 36 kGy from the bottom to the upper line at the wavelength of 533 nm.

protons were generated, and therefore, the absorption of the C6 proton adduct ($C6H^+$) appeared at 533 nm. With increasing absorbed dose, the absorption intensity of $C6H^+$ increased, and the absorption intensity of neutral C6 at 460 nm decreased simultaneously, with a clear isosbestic point at 497 nm. Here, it is important to point out that the total amount of C6 is conserved during the film radiolysis, for example, 16% of the initial neutral C6 converts to acid form $C6H^+$ after exposure at 36 kGy and the remaining neutral C6 is about 82%. The total is 98%, or complete conservation within measurement error. This conservation of C6 appeared to hold true for all of the experiments of this study.

In Figure 4a, we plot the 533 nm absorbance of $C6H^+$ versus the initial weight fraction of C6 for films irradiated to 30 kGy.

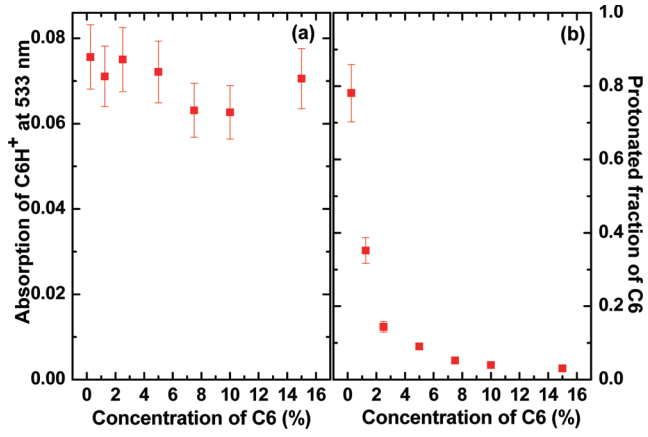

Figure 4. $C6H^+$ formation in PHS films with 10 wt % $Ph_3S^+TfO^-$. Virtually no effect of the C6 indicator is seen, up to 15% C6 by weight. (a) $C6H^+$ (acid yield) versus C6 concentration; (b) fraction of $C6H^+$ versus C6 concentration.

There is virtually no change in the total acid produced for C6 from 0.25 to 15% by weight. The protonated fraction of indicator (i.e., $[C6H^+]/([C6H^+]+[C6])$) is plotted in Figure 4b. Assuming that the total acid produced is constant in these films, the C6 indicator has not been saturated, even up to 80% of the acid form. (Of course, a larger dose can saturate the indicator.) The implication of both Figures 3 and 4 is that the C6 does not perturb the radiation-induced reactions except by scavenging protons to form $C6H^+$. Initial radical cations of the C6 must form and presumably rapidly transfer the electron "hole" to a more stable location.

$$C6^+ + (Ar{-}OH) \rightarrow (Ar{-}OH)^+ + C6 \quad (6)$$

Coumarins are also known to be good electron scavengers. The evidence suggests that any C6 anion will inevitably transfer its electron to Ph_3S^+, which is present at high concentration.

$$C6^- + Ph_3S^+ \rightarrow C6 + Ph_2S + Ph^{\bullet} \quad (7)$$

This conclusion is consistent with the EPR evidence presented earlier.

The acid density (mmol kg^{-1}) was calculated from the acid indicator spectra before and after exposure using the following equation derived from the Lambert–Beer law, $N_m = 1000\Delta OD/(N_A \times \varepsilon \times \rho \times l)$. Here, N_m, ΔOD, N_A, ε, ρ, and l are the molar acid density (mmol kg^{-1}), the optical density change at 533 nm, Avogadro's constant, the molar extinction coefficient of $C6H^+$ in the PHS film, the film density, and the thickness, respectively. The calculated acid densities are plotted versus the absorbed dose in Figure 5a (□ original). A good

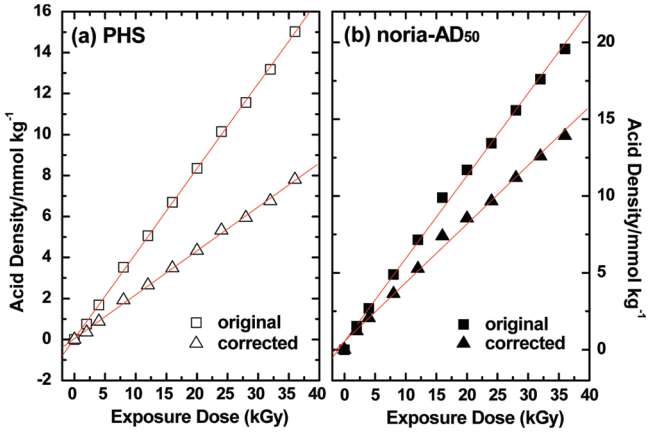

Figure 5. Acid generation efficiencies in (a) PHS and (b) noria-AD_{50} films with 10 wt % $Ph_3S^+TfO^-$ and 5 wt % C6, respectively, on silica substrates. The apparent acid G values of PHS (□) and noria-AD_{50} (■) films are determined from the slopes to be 3.9 and 5.1, respectively. The G values after correction for the substrate contribution are determined to be 2.5 (Δ) and 3.2 (▲), respectively.

linearity was observed in the relationship between the acid densities and absorbed dose. (The linear dependence suggests a homogeneous dispersion of the polymer/$Ph_3S^+TfO^-$/C6 system without phase separation, which is of general concern in thin resist films.[45−47]) The apparent G value of the acid generation (molecules of acid generated by 100 eV of absorbed energy) was evaluated from the slope in Figure 5a (□ original) to be 3.9 ± 0.4.

This apparent G value is much higher than 2.3 protons per 100 eV reported previously by Nakano et al.[20] It is highly unlikely that protons are generated through any chain reaction or other mechanisms in PHS/$Ph_3S^+TfO^-$ films. In the electron beam lithography of PHS films on silica, it was reported that the electrons backscattered from the fused quartz substrates may give a contribution to the acid generation.[25] It is also well-established that triplet excitons in fused silica have a long lifetime and may move over long distances.[19] Therefore, it is reasonable to assume that the energy deposited in the substrates by γ-radiolysis may transfer to the surface and

dx.doi.org/10.1021/jp300677q | J. Phys. Chem. B 2012, 116, 6215−6224

contribute to the acid generation via the excited-state chemistry of the Ph_3S^+ cation.[48−50] The film thickness dependence upon acid generation has been investigated to quantify this effect.

3.3. Thickness Dependence of Acid Generation Efficiency in PHS Films. The film thickness was varied by diluting the original casting solution. Because relatively thinner films were prepared by the dilute casting solution, the same ratio of PHS, $Ph_3S^+TfO^-$, and C6 in the film could be retained. Therefore, the film thickness and acid generation can be characterized by absorptions of the neutral C6 and $C6H^+$, respectively. Absorption of the C6 at 533 nm before irradiation is proportional to the film thickness. For a given dose, the absorption of $C6H^+$should linearly increase with increasing film thickness, and the intercept of the fitting line should be zero (at zero film thickness) if there is no contribution to acid generation from the energy deposited in the substrates.

In fact, the intercept of the plot is positive rather than zero, as shown in Figure 6a, although a linear dependence on

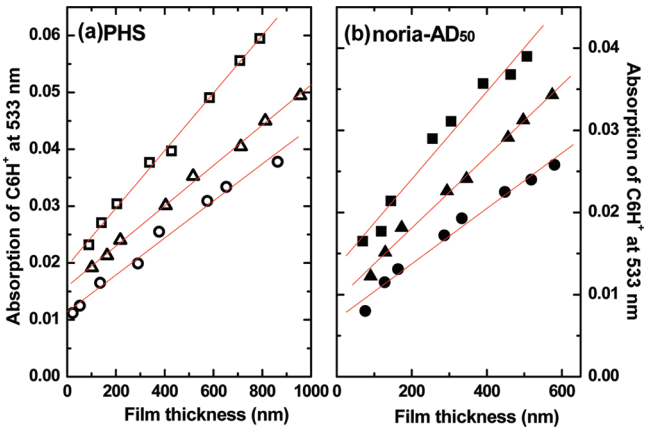

Figure 6. Film thickness dependences of the acid generation of $Ph_3S^+TfO^-$ after exposure at 12 kGy with different concentrations of acid generator $Ph_3S^+TfO^-$: (a) PHS films; (b) noria-AD_{50} films. Concentrations of $Ph_3S^+TfO^-$ are 5 (○,●), 10 (Δ,▲), and 15 wt % (□,■), respectively.

thickness was obtained when the films were irradiated to 12 kGy. The large positive intercept implies that the deposited energy in the substrate definitely has contribution to the acid generation near the silica/film interface. If we want to get the real acid generation efficiency from the neat bulk film by direct incident radiation, the substrate contribution to the acid yield should be subtracted. Considering the linear relationship between total acid production and absorbed dose, the positive intercepts must be proportional to the absorbed dose as well. Thus, the positive intercepts at other different doses are calculated to correct the acid densities at their respective doses. The corrected acid densities are displayed in Figure 5a (Δ corrected). The corrected G value is estimated to be 2.5 ± 0.3 per 100 eV from the slope.

Clearly, the present corrected result and the G value of 2.3/100 eV previously reported by Nakano et al. are in good agreement.[20] The method of Nakano et al. involved dissolving the film in a fixed amount of solvent and measuring the total acid produced via a pH meter. We have also experimented with this method. By our experience, the procedure introduced here using an acid indicator with the variation of film thickness on the fused silica substrate is more precise. Its accuracy depends on the extinction coefficient used for $C6H^+$ and on the estimated film density, which are both known to well within 10%.

Because the substrate has significant contribution to the acid production in the films, different substrates might give different contributions, and therefore, the uncorrected acid yields would be changed significantly. The radiolysis of PHS films on borosilicate glass (Pyrex) substrate was performed to demonstrate this. However, it should be pointed out that the Pyrex has a significant disadvantage as a film substrate. When undergoing γ-radiolysis, the Pyrex substrates become darker and nontransparent with increasing dose, resulting in less reliable baselines for the film spectra. A blank slide baseline was collected with every run in order to correct the absorption spectra. The changing baselines made measurement less convenient and less accurate.

As shown in Figure 7a and b, the acid yields (represented by ΔOD at 533 nm) of the films on the Pyrex glasses were found to be much lower than those on fused silica substrates no matter what the thickness of the film. The intercept is zero within error. The acid yield on Pyrex substrates without any correction is determined to be 2.3 ± 0.2 per 100 eV, as shown in Figure 7c, which is in good agreement with that on silica after correction. This indicates that the Pyrex glass substrates make almost no contribution to the acid production.

3.4. Acid Distribution within the PHS Films. In the radiolysis of the PHS films, it is experimentally demonstrated that energy deposited in the silica substrates transfers to the PHS/silica interface and contributes significantly to the acid yields. Therefore, it is reasonable to assume that the acid distribution could not be uniform from the interface to the bulk film due to the distance limitation of energy transfer.

The actual acid concentration can be measured as a fraction of $C6H^+$ absorbance relative to the total absorbance of both C6 and $C6H^+$. This quantity is plotted in Figure 8 for the data found in Figure 6. It is clear that for thin films, the fraction of protonated C6 is much higher than that for thick films. For example, the acid yield in terms of the protonated C6 fraction near the interface (the film thickness is about 80 nm) is 0.18, which is much higher than a fraction of 0.04 with a thickness of 680 nm, as shown in Figure 8a.

Most importantly, it is seen that the acid yields increase sharply at the interface with the increasing concentration of $Ph_3S^+TfO^-$ but are nearly independent of $Ph_3S^+TfO^-$ in the bulk. This insight is not immediately available from the plot in Figure 6. The increasing concentration of $Ph_3S^+TfO^-$ enhances proton production via the energy transferred at the PHS/silica interface. However, in the bulk film, the acid yields are almost constant whatever the concentration of $Ph_3S^+TfO^-$, as shown in Figure 8a.

3.5. Acid Generation Efficiency of Noria-AD_{50} Films. The noria-AD_{50} films were also prepared with 10 wt % $Ph_3S^+TfO^-$ and 5 wt % C6. By exposure to γ-radiation, the generation of acid results in the conversion of C6 to the $C6H^+$, as displayed in Figure 3b. Similar to the PHS films, the isosbestic point of spectra after radiolysis was found at 488 nm. On the basis of the Lambert−Beer law, the estimated film density of 1.1 ± 0.1 g cm^{-3}, and the extinction coefficients of the noria-AD_{50} film, the acid densities were calculated and plotted in Figure 5b (■ original). The acid densities versus absorbed dose exhibit good linearity. The G value for acid production in the noria-AD_{50} films was estimated from the initial dose dependence to be 5.1 ± 0.5 per 100 eV.

dx.doi.org/10.1021/jp300677q | J. Phys. Chem. B 2012, 116, 6215−6224

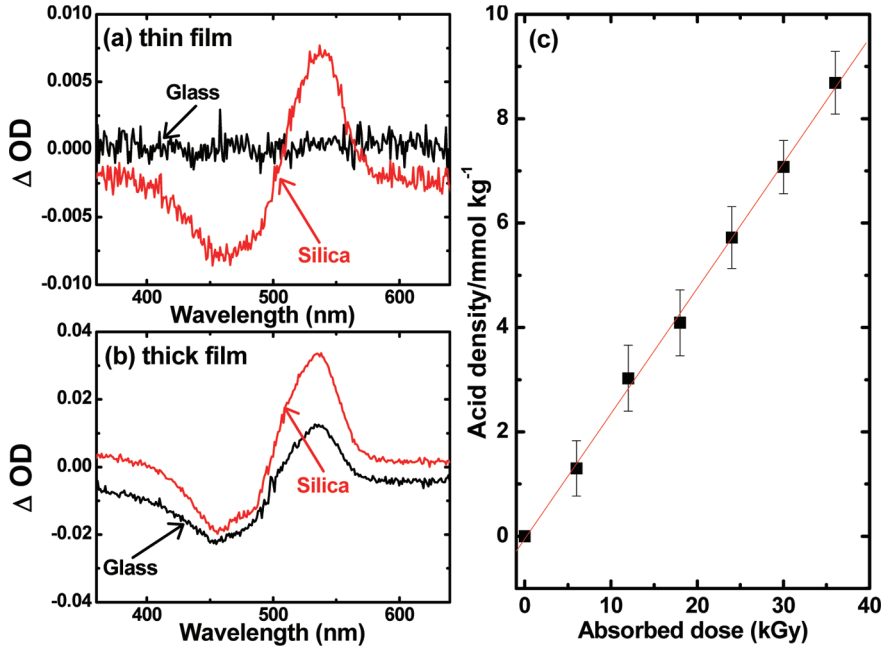

Figure 7. Difference spectra of PHS films on glass and fused silica substrates with 10 wt % $Ph_3S^+TfO^-$ and 5 wt % C6. (a,b) Absorption spectra of thin and thick films after radiolysis at 6 kGy; (c) acid production of the PHS film on the Pyrex borosilicate glass substrate with a thickness of about 900 nm.

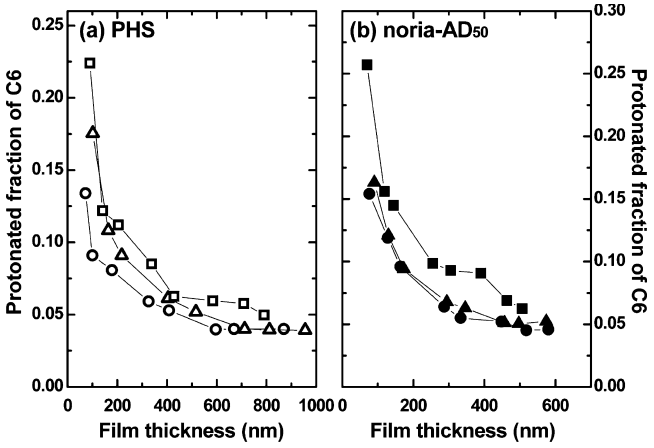

Figure 8. The protonated fraction of C6 indicator as a function of the film thickness. The data are same as those plotted in Figure 3. (a) PHS films; (b) noria-AD_{50} films.

Similar to the PHS films, the thickness dependence of acid generation was investigated to quantify the substrate contribution. Figure 6b shows that plotting of $C6H^+$ absorption versus the thickness is linear and has a positive intercept that depends on the $Ph_3S^+TfO^-$ concentration. The acid densities were corrected for the substrate contribution in the same way as with PHS films and are shown in Figure 5b (▲ corrected). The *G* value is corrected from 5.1 ± 0.5 to 3.2 ± 0.3 per 100 eV. The acid distribution of the noria-AD_{50} film is also determined and is similar to that of the PHS film, as shown in Figure 8b. Similarly, the acid yields at the noria-AD_{50}/silica interface are higher than those of the bulk film, and the acid yields are constant with different concentrations of $Ph_3S^+TfO^-$ in the bulk films.

Acid generation in noria-AD_{50} differs in at least one significant way from that of PHS. When we irradiate a film of PHS/C6 without adding any of the $Ph_3S^+TfO^-$, we have no generation of $C6H^+$ absorbance. When we do the same "blank" experiment using noria-AD_{50}, we do get a small absorbance from $C6H^+$, corresponding to a *G* value for acid production of 0.34 molecules/100 eV, or around 10% of the value in the presence of $Ph_3S^+TfO^-$. (Data are presented in Figure 3S of the Supporting Information.)

Generation of protons in noria-AD_{50} from the cation radicals via reaction 4 is to be expected. The surprise is that the protons have not recombined with the electrons or with some product anion, as clearly happens in PHS. It was suggested in section 3.1 that electrons might be captured by the ester group in noria-AD_{50}, producing noria-carboxylate and 2-methyladamantyl radical. There seems to be no other simple mechanism by which to explain the existence of any $C6H^+$ in our blank experiment. The adamantyl radicals were surprisingly not found in the 77 K EPR experiment (see section 3.1). We have to postulate that the adamantyl radicals can extract H atoms from noria-AD_{50} to produce the noria-$O^\bullet$ radical at 77 K or else are completely recombined with excess H atoms. Assuming that the anion product is a carboxylate group, we still have to ask why $C6H^+$ is observed because the pK_a of $C6H^+$ is 1.6[51] and that of any carboxylate anion should be around 4. The only answer that makes sense is that C6 constitutes a proton trap, and once $C6H^+$ is formed, it is no longer possible for the proton to migrate through the matrix to recombine with any carboxylate anions.

We can certainly conclude that the electron capture by ester groups is of minor importance in noria-AD_{50} lithography films when $Ph_3S^+TfO^-$ is present. Acid generation efficiency is insensitive to the Ph_3S^+ concentration in noria-AD_{50}, implying that virtually all electrons are scavenged by this reagent present at 5−10% by weight.

3.6. Acid Yields of PHS Films in the Ambient Air. In EUV lithography, the film exposure must be performed under vacuum due to the absorption of the EUV photons by an atmosphere. In the present study, we used γ-rays to replace the

dx.doi.org/10.1021/jp300677q | J. Phys. Chem. B 2012, 116, 6215−6224

EUV exposure tool, and the film irradiation can equally well be performed in the ambient air. Our initial acid generation experiments in PHS were designed to duplicate γ-radiolysis results of Nakano et al., who report experiments carried out in air.[20] However, as we describe below, the results are quite different from those obtained under argon. We report these experiments as a cautionary note for future workers and emphasize the importance of using an inert environment. The section is not important for the comparison between PHS and noria-AD_{50}.

Figure 9a shows the different absorption spectra of identical PHS films irradiated at 12 kGy under argon (blue line) and air

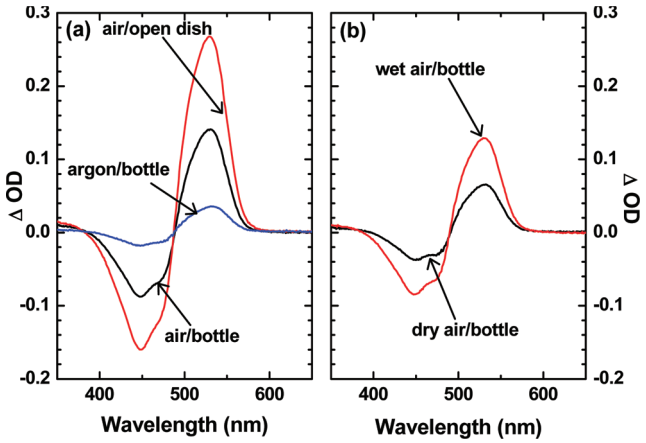

Figure 9. Difference spectra of PHS films with 10 wt % $Ph_3S^+TfO^-$ and 5 wt % C6 irradiated to 12 kGy: (a) in the bottle sealed with argon or air and in the open dish; (b) in the bottle sealed with wet and dry air, respectively.

(black line) atmospheres in the sealed flask, respectively. In the argon case, the ΔOD was merely 0.034 at 533 nm; in contrast, the ΔOD of 0.270 was much larger for the irradiated films in the ambient air, suggesting G values on the order of 20 per 100 eV! Thickness dependence for the PHS films under air showed an intercept much larger than those in Figure 6, suggesting some large effect of the air/film interface. A film made without acid generator $Ph_3S^+TfO^-$ was irradiated under air and also gave a large $C6H^+$ signal. Films were irradiated under pure nitrogen and oxygen, respectively, and the acid production was found to be almost the same as that with the argon atmosphere. Taken together, all of the evidence indicates that the acid must be generated in the air and then deposited on the film surface. Considering that the pK_a of $C6H^+$ is 1.6,[51] the acid must be a strong mineral acid. Of acids that might be generated in air, only nitric acid seems to be strong enough to explain the observation. Ultimately, we extracted an air-irradiated film with 1.0 mL of water. The strong color from $C6H^+$ decreased, and ion chromatography established the presence of significant NO_3^- in the extract (as well as triflate).

In fact, it is well-established that nitric acid is a major initial product in the irradiation of moist air.[52,53] According to Jones, when moisture is present in a N_2/O_2 mixture, nitric acid and NO_2 are formed by irradiation until the water present is exhausted. Subsequently, the nitric acid decreases with the regeneration of H_2O, and the NO_2 product continues to grow. Therefore, water renewal is critical to efficient acid generation. Figure 9b shows that the acid yields of films irradiated in the wet (saturated by bubbling) air are about two times ($\Delta OD_{533\ nm}$: 0.13 vs 0.065) higher than that in the "dry" air. We found very significant variation in the acid production depending on whether the irradiations occurred in an open flask or an open dish. The air circulation is apparently more efficient in the open dish than that in the flask, and efficient air renewal facilitates the acid generation.

Given all of our difficulties with the measurements on PHS films in a typical ambient air environment, we can only wonder how the experiments reported by Nakano et al.[20] produced a successful result. The "atmosphere" that they used must have been either extremely dry air or not air at all.

4. DISCUSSION

The basic quantitative result of this comparative study of acid generation in PHS and noria-AD_{50} lithography films is that the yield in noria-AD_{50} (3.2/100 eV) is somewhat larger than in PHS (2.5/100 eV), for similar loading of the photoacid generator $Ph_3S^+TfO^-$. This could have important technological implication because it indicates that the noria-based EUV films may require smaller exposure doses of EUV light to generate the same amount of acid. The important question, for future development, is why the noria films are superior for acid production.

The EPR study is consistent with the model of chemistry in phenolic matrixes, which was developed previously. At 77 K, trapped yields of the aryloxy radical of 5.7/100 eV in noria-AD_{50} and 7.1/100 eV in PHS are significantly larger than the acid yields determined at room temperature, as they must be. Only a fraction of the excess aryloxy yield seems to be accounted for by a H atom geminate partner. The remaining aryloxy radical should be generated by the phenyl radicals from Ph_3S^+ dissociation. In principle, one could expect the aryloxy radical yield at 77 K to be over twice the acid yield (via reactions 4 and 5). However, it is also possible for the phenyl radicals to geminately recombine with either H atoms or aryloxy, reducing the radical yield below twice the acid yield. It is surprising that upon warming to room temperature, the aryloxy yields became so much smaller (~10×) than the acid yields. The implication is that a large fraction of aryloxy radical−radical recombination/diproportionation occurs within the first minute at room temperature. This is not inconsistent with the (nearly) stretched exponential decay kinetics observed at much longer time and the deviation from stretched exponential kinetics at short time that we ascribe to geminate recombination.

An assumption of the present comparison is that ionization potentials of the two materials are the same. For a lower ionization potential, more of the available energy could go into ionization rather than electronic excitation and ultimate heat dissipation, producing more ($hole^+$,e^-) charge pairs. The gas-phase adiabatic ionization potential of phenol is 8.5 eV, whereas that of resorcinol is 8.3 eV.[54] Forming an ester of one of the resorcinol OH groups actually increases the ionization potential slightly.[55] Forming a water hydrogen bond to the phenol OH reduces the ionization potential by 0.54 eV in vacuum.[56] No free OH is apparent in the infrared spectra of the films; therefore, we expect that these OH groups are hydrogen bonded in both matrixes. (See the Supporting Information.) On the basis of these comparisons, we might expect the noria-AD_{50} ionization potential to be very slightly lower than the PHS ionization potential. It is not clear that this is enough to produce a 25% difference in the acid yields in the two matrixes.

dx.doi.org/10.1021/jp300677q | J. Phys. Chem. B 2012, 116, 6215−6224

Another possibility for effective reduction of the ionization potential is a charge-transfer electronic transition. If the noria-AD_{50} were to couple to the Ph_3S^+, electronic excitation might stimulate a proton-coupled electron transfer. This process would bypass the need to actually ionize the matrix and produce quasi-free electrons, just as in solution-phase charge-transfer-to-solvent transitions.[57] We have closely compared the UV spectra of PHS/ and noria-AD_{50}/$Ph_3S^+TfO^-$ mixtures in films and dilute solution, but we find no evidence of a new band that might be ascribed to such a transition. (See spectra in the Supporting Information.)

Our study showed that the $Ph_3S^+TfO^-$ concentration at 5 or 10% by weight was not a limiting factor in the acid production (cf. Figure 5). It appears that essentially all of the electrons liberated from the matrix are captured by Ph_3S^+ in both materials. Electron capture by ester groups in the noria-AD_{50} was shown to be unimportant in the presence of $Ph_3S^+TfO^-$. Nevertheless, some electrons must recombine with cations in very early events that cannot be intercepted by the Ph_3S^+. One might suppose that if electron capture is not limiting, perhaps hole migration and dissociation are critical. Natsuda et al. have shown that in PHS, the hole dissociation giving an aryloxy radical and proton is extremely fast because virtually all OH groups are hydrogen-bonded.[58] The same must certainly be true in the noria-AD_{50} matrix as we can detect significant H-bonded water even after baking the film material and redissolving for NMR analysis. No free OH is apparent in the infrared spectra of the films. (See the Supporting Information.) A simple calculation shows that the density of −ArOH groups in noria-AD_{50} is 3.7 mmol g^{-1}, whereas in PHS, the density is 8.0 mmol g^{-1}. If the kinetics of hole capture at the aromatic ring is limiting, we would expect the yield in PHS to be higher than that in noria-AD_{50}.

The reason for the slightly larger yield in noria-AD_{50} is almost certainly found in a previous study[59] of acid yield in PHS films where the phenolic OH groups were protected with methyl, *t*-butyl, or adamantyl groups up to a certain fraction (i.e., ArOH was changed to ArOX, where X is the alkyl group). In the case of methyl or *t*-butyl protection, the acid yield decreased linearly with the substitution fraction. When adamantyl groups were used, the acid yield actually increased linearly with the substitution. The special behavior of adamantyl in this experiment may be explained by the very high acidity that was determined for the adamantyl cation.[60] The pK_a of the adamantyl radical cation is estimated to be −12, making it even more acidic than the phenol radical cation. Nevertheless, one has to postulate that the speed of the adamantyl deprotonation/rearrangement competes favorably with the speed of proton transfer in the hydrogen-bonded phenol case. It is difficult to imagine how this happens efficiently except by proton transfer to the oxygen atoms binding the adamantyl group to the polymer. When we add the density of adamantyl groups to the density of Ar−OH groups in noria-AD_{50}, the total 7.4 mmol g^{-1} is quite similar to 8.0 mmol g^{-1} of PHS. The similarity of acid yields in the two matrixes is therefore rationalized.

5. CONCLUSION

The mechanism of acid production in noria-AD_{50} molecular glass films containing $Ph_3S^+TfO^-$ was investigated and appears to be very similar to that of PHS polymer films. In both cases, γ-irradiation at 77 K followed by EPR detection showed the production of substituted aryloxy radicals and H atoms. The H atoms recombined upon warming, but substantial aryloxy radical signal persisted at room temperature for many days, roughly following stretched exponential decay kinetics.

Using PHS films as a test system, a new procedure of acid yield measurement in EUV lithography films was developed for the γ-irradiation source. The procedure provides a precise determination of the fused silica substrate contribution to the total acid yields by changing the film thickness. The acid yield in PHS film with 10 wt % $Ph_3S^+TfO^-$ is determined to be 2.5 per 100 eV of radiation energy. Similarly, the yield in thin films of noria-$AD_{50}$with 10 wt % of $Ph_3S^+TfO^-$ was found to be 3.2 per 100 eV. In noria-AD_{50}, dissociative electron capture by the ester groups was found to be a minor process.

The slightly higher acid yield in noria-AD_{50} is difficult to reconcile with the 50% lower concentration of Ar−OH groups in noria-AD_{50} compared to that in PHS. Previous work in PHS has shown that protection of the OH groups with methyl or *t*-butyl reduces the acid yield proportional to the protection fraction. However, protection by adamantyl enhances the acid production.[59] In the noria-AD_{50}, we postulate that cations formed on 2-methyladamantyl transfer a proton to the ester carbonyl oxygen on a time scale similar to proton transfer of H-bonded phenol protons. The relaxation makes ultrafast recombination with the electron less likely.

■ ASSOCIATED CONTENT

Supporting Information

Figures showing UV−vis absorption and IR spectra of the PHS and noria-AD_{50} films. This material is available free of charge via the Internet at http://pubs.acs.org.

■ AUTHOR INFORMATION

Corresponding Author

*E-mail: bartels.5@nd.edu. Phone: (574) 631-5561. Fax: (574) 631-8068.

Notes

The authors declare no competing financial interest.

■ ACKNOWLEDGMENTS

This work was funded by a grant from the Intel Corporation. The authors thank Dr. James Blackwell of Intel for his continuous interest and for comments on the manuscript in preparation. We gratefully acknowledge the gift of the noria-AD_{50} sample from Dr. Hiroki Nakagawa of JSR Micro, Inc. We thank Dr. Jay Laverne for ion chromatography analysis. The use of the facilities at the Notre Dame Radiation Laboratory, which is supported by the Division of Chemical Sciences, Geosciences, and Biosciences, Office of Basic Energy Sciences of the U.S. Department of Energy through Award DE-FC02-04ER15533, in the performance of this research is gratefully acknowledged. This is document number NDRL-4909.

■ REFERENCES

(1) Wallraff, G.; Hinsberg, W. *Chem. Rev.* **1999**, *99*, 1801−1821.
(2) Mack, C. A. *Fundamental Principles of Optical Lithography: The Science of Microfabrication*; Wiley: West Sussex, England, 2008.
(3) Reichmanis, E.; Thompson, L. *Chem. Rev.* **1989**, *89*, 1273−1289.
(4) Macdonald, S.; Willson, C.; Frechet, J. *Acc. Chem. Res.* **1994**, *27*, 151−158.
(5) Sanders, D. P. *Chem. Rev.* **2010**, *110*, 321−360.
(6) Ito, H. *Adv. Polym. Sci.* **2005**, *172*, 37−245.
(7) Kozawa, T.; Tagawa, S. *Jpn. J. Appl. Phys.* **2010**, *49*, 030001.

(8) Yamaguchi, T.; Yamazaki, K.; Namatsu, H. *Adv. Resist Mater. Process. Technol.* **2003**, *5039*, 1212−1219.
(9) Yamaguchi, T.; Yamazaki, K.; Namatsu, H. *J. Vac. Sci. Technol., B* **2004**, *22*, 2604−2610.
(10) Patsis, G. P.; Gogolides, E.; Van Werden, K. *Jpn. J. Appl. Phys., Part 1* **2005**, *44*, 6341−6348.
(11) Shiraishi, H.; Yoshimura, T.; Sakamizu, T.; Ueno, T.; Okazaki, S. *J. Vac. Sci. Technol., B* **1994**, *12*, 3895−3899.
(12) Dai, J.; Chang, S. W.; Hamad, A.; Yang, D.; Felix, N.; Ober, C. K. *Chem. Mater.* **2006**, *18*, 3404−3411.
(13) Kudo, H.; Hayashi, R.; Mitani, K.; Yokozawa, T.; Kasuga, N. C.; Nishikubo, T. *Angew. Chem., Int. Ed.* **2006**, *45*, 7948−7952.
(14) Kimura, T.; Nishino, K.; Shimizu, M.; Hirai, Y.; Maruyama, K.; Kai, T. *J. Photopolym. Sci. Technol.* **2010**, *23*, 643−648.
(15) Nishikubo, T.; Kudo, H.; Suyama, Y.; Oizumi, H.; Itani, T. *J. Photopolym. Sci. Technol.* **2009**, *22*, 73−76.
(16) Kudo, H.; Jinguji, M.; Nishikubo, T.; Oizumi, H.; Itani, T. *J. Photopolym. Sci. Technol.* **2010**, *23*, 657−664.
(17) Kudo, H.; Suyama, Y.; Oizumi, H.; Itani, T.; Nishikubo, T. *J. Mater. Chem.* **2010**, *20*, 4445−4450.
(18) Ito, H.; Willson, C. *Polym. Eng. Sci.* **1983**, *23*, 1012−1018.
(19) Kozawa, T.; Nagahara, S.; Yoshida, Y.; Tagawa, S.; Watanabe, T.; Yamshita, Y. *J. Vac. Sci. Technol., B* **1997**, *15*, 2582−2586.
(20) Nakano, A.; Kozawa, T.; Okamoto, K.; Tagawa, S.; Kai, T.; Shimokawa, T. *Jpn. J. Appl. Phys., Part 1* **2006**, *45*, 6866−6871.
(21) Okamoto, K.; Kozawa, T.; Natsuda, K.; Seki, S.; Tagawa, S. *J. Phys. Chem. B* **2008**, *112*, 9275−9280.
(22) Bordwell, F.; Cheng, J. *J. Am. Chem. Soc.* **1991**, *113*, 1736−1743.
(23) Howells, R.; Mccown, J. *Chem. Rev.* **1977**, *77*, 69−92.
(24) Note that 92 eV is well above the bound−bound valence transitions of molecular materials but well below the K edge for carbon and oxygen. The overwhelming transition probability is bound-free (i.e., ionization). The probability for the electronic excitation (nonionized) of a typical resist matrix upon exposure to 92.5 eV photons does not significantly differ from that of several keV photons or electrons (ref 7).
(25) Yamamoto, H.; Kozawa, T.; Nakano, A.; Okamoto, K.; Yamamoto, Y.; Ando, T.; Sato, M.; Komano, H.; Tagawa, S. *Jpn. J. Appl. Phys., Part 2* **2004**, *43*, L848−L850.
(26) Pohlers, G.; Scaiano, J.; Sinta, R. *Chem. Mater.* **1997**, *9*, 3222−3230.
(27) Fricke, H.; Hart, E. *J. Chem. Phys.* **1935**, *3*, 60−61.
(28) Weir, N.; Arct, J.; Farahani, M. *Polym. Degrad. Stab.* **1985**, *13*, 361−375.
(29) Porter, G.; Wright, F. *Trans. Faraday Soc.* **1955**, *51*, 1469−1474.
(30) Jinot, C.; Madden, K.; Schuler, R. *J. Phys. Chem.* **1986**, *90*, 4979−4981.
(31) Brede, O.; Orthner, H.; Zubarev, V.; Hermann, R. *J. Phys. Chem.* **1996**, *100*, 7097−7105.
(32) Dixton, W.; Murphy, D. *J. Chem. Soc., Faraday Trans. 2* **1976**, *72*, 1221−1230.
(33) Kohler, G.; Kittel, G.; Getoff, N. *J. Potochem.* **1982**, *18*, 19−27.
(34) Kasai, P.; Hedaya, E.; Whipple, E. *J. Am. Chem. Soc.* **1969**, *91*, 4364−4368.
(35) Bennett, J.; Mile, B.; Thomas, A. *Chem. Commun.* **1965**, *12*, 265−267.
(36) Bennett, J.; Mile, B.; Thomas, A. *Proc. R. Soc. London, Ser. A* **1966**, *293*, 246−258.
(37) Uppalapati, S.; Chada, S.; Engelhard, M. H.; Yan, M. *Macromol. Chem. Phys.* **2010**, *211*, 461−470.
(38) Stepanov, A.; Tkatchenko, V.; Bolshakov, B.; Tolkatchev, V. *Int. J. Chem. Kinet.* **1978**, *10*, 637−648.
(39) Siebrand, W.; Wildman, T. *Acc. Chem. Res.* **1986**, *19*, 238−243.
(40) Phillips, J. *Rep. Prog. Phys.* **1996**, *59*, 1133−1207.
(41) Metzler, R.; Klafter, J.; Jortner, J.; Volk, M. *Chem. Phys. Lett.* **1998**, *293*, 477−484.
(42) Bussandri, A.; van Willigen, H. *J. Phys. Chem. A* **2002**, *106*, 1524−1532.
(43) King, G. A.; Oliver, T. A. A.; Nix, M. G. D.; Ashfold, M. N. R. *J. Phys. Chem. A* **2009**, *113*, 7984−7993.
(44) Sevilla, M.; Morehouse, K.; Swarts, S. *J. Phys. Chem.* **1981**, *85*, 923−927.
(45) VanderHart, D.; Prabhu, V.; Lin, E. *Chem. Mater.* **2004**, *16*, 3074−3084.
(46) VanderHart, D. L.; Prabhu, V. M.; Lavery, K. A.; Dennis, C. L.; Rao, A. B.; Lin, E. K. *J. Magn. Reson.* **2009**, *201*, 100−110.
(47) VanderHart, D. L.; Prabhu, V. M.; De Silva, A.; Felix, N. M.; Ober, C. K. *J. Mater. Chem.* **2009**, *19*, 2683−2694.
(48) Shkrob, I.; Trifunac, A. *Phys. Rev. B: Condens. Matter* **1996**, *54*, 15073−15078.
(49) Shkrob, I.; Trifunac, A. *J. Chem. Phys.* **1997**, *107*, 2374−2385.
(50) Dektar, J.; Hacker, N. *J. Org. Chem.* **1988**, *53*, 1833−1835.
(51) Corrent, S.; Hahn, P.; Pohlers, G.; Connolly, T.; Scaiano, J.; Fornes, V.; Garcia, H. *J. Phys. Chem. B* **1998**, *102*, 5852−5858.
(52) Jones, A. *Radiat. Res.* **1959**, *10*, 655−663.
(53) Spinks, J. W. T.; Woods, R. J. *An Introduction to Radiation Chemistry*; Wiley Interscience: New York, 1990; p 217.
(54) Gerhards, M.; Unterberg, C.; Schumm, S. *J. Chem. Phys.* **1999**, *111*, 7966−7975.
(55) Benezra, S.; Bursey, M. *J. Chem. Soc. B* **1971**, *7*, 1515−1520.
(56) Lipert, R.; Colson, S. *J. Chem. Phys.* **1990**, *92*, 3240−3241.
(57) Blandamer, M. J.; Fox, M. F. *Chem. Rev.* **1970**, *70*, 59−93.
(58) Natsuda, K.; Kozawa, T.; Okamoto, K.; Saeki, A.; Tagawa, S. *Adv. Resist Mater. Process. Technol.* **2010**, *7639*, 76391K.
(59) Yamamoto, H.; Kozawa, T.; Nakano, A.; Okamoto, K.; Tagawa, S.; Ando, T.; Sato, M.; Komano, H. *J. Vac. Sci. Technol., B* **2004**, *22*, 3522−3524.
(60) Mella, M.; Freccero, M.; Soldi, T.; Fasani, E.; Albini, A. *J. Org. Chem.* **1996**, *61*, 1413−1422.